Electronic Supplementary Material (ESI) for RSC Advances.

A molecular cobalt catalyst supported by an amine-bis(phenolate) ligand for both electrolytic and photolytic water reduction

Ling-Zhi Fu, Ling-Ling Zhou and Shu-Zhong Zhan*

College of Chemistry and Chemical Engineering, South China University of Technology, Guangzhou 510640, China.

Supplementary Materials

Table of context

8	**Fig. S8.** GC traces after a 2-h controlled-potential electrolysis at −1.45 V *vs* Ag/AgCl of 4.0 μM complex **1** in DMF with 3.4 mM acid. A standard of CH_4 was added for calibration purposes.
9	**Fig. S9.** Turnover frequency (mol H_2/mol catalysts/h) for electrocatalystic hydrogen production by complex **1** (0.25 μM) under a series of overpotentials.
10	**Fig. S10.** (a) GC traces after a 1-h controlled-potential electrolysis at −1.45 V *vs* Ag/AgCl of 2.0 μM complex **1** in 0.25 M phosphate buffer, pH 7.0. A standard of CH_4 was added for calibration purposes. (b) Measured (black) and calculated (red) pH changes assuming a 100% Faradic efficiency of complex **1** during electrolysis. (the theoretical pH change over time can be calculated by the equation of $pH = 14 + \lg\frac{\sum It}{FV}$ where I = current (A), t = time (s), F = Faraday constant (96485 C/mol), V = solution volume (0.04 L)).
11	**Fig. S11.** Turnover frequency (mol H_2/mol catalysts/h) for electrocatalystic hydrogen production by complex **1** (2.0 μM) under a series of overpotentials (mV) at pH 7.0.
12	**Fig. S12.** EDS of a glassy carbon electrode after 3 h electrolysis. There was no significant change in the EDS after a 3 h electrolysis period.
13	**Fig. S13.** (a) Extended controlled potential electrolysis of 4.5 μM complex **1**, showing charge buildup versus time with an applied potential of -1.45 V versus Ag/AgCl. (b) Catalytic current obtained upon controlled potential electrolysis with 4.5 μM complex **1**. Conditions: 0.25 M buffer solution, pH 7.0, GC working electrode (1.25 cm^2), Ag/AgCl in saturated KCl reference electrode, Pt wire counter electrode, 60 h.
14	**Fig. S14.** Effect of pHs on different photocatalytic systems, containing 0.70 mM $Ru(bpy)_3Cl_2$, 0.08 M ascorbic acid and 0.10 mM complex **1**, under air.
15	**Fig. S15.** Effect of addition of $Ru(bpy)_3Cl_2$ on different photocatalytic systems, containing 0.15 M ascorbic acid and 0.10 mM complex **1** at pH 6.0.
16	**Fig. S16**. Effect of addition of ascorbic acid on different photocatalytic systems, containing 0.70 mM $Ru(bpy)_3Cl_2$ and 0.10 mM **1,** at pH 6.0.
17	**Fig. S17.** Hydrogen evolution kinetics obtained upon continuous visible irradiation (λ = 469 nm) of 1.0 M buffer pH 6.0 solutions (4 mL) containing 0.90 mM $Ru(bpy)_3Cl_2$, 0.15 M ascorbic acid, and **1** at 0.02 mM (a), 0.05 mM (b), and 0.10 mM (c) concentration.
18	**Fig. S18**. Hydrogen evolution obtained upon continuous visible irradiation (λ = 469 nm) of pH 6.0 solutions (4 mL) containing 0.90 mM $Ru(bpy)_3Cl_2$, 0.15 M ascorbic acid, and 0.10 mM complex **1** under Ar (black trace), and air (red trace).

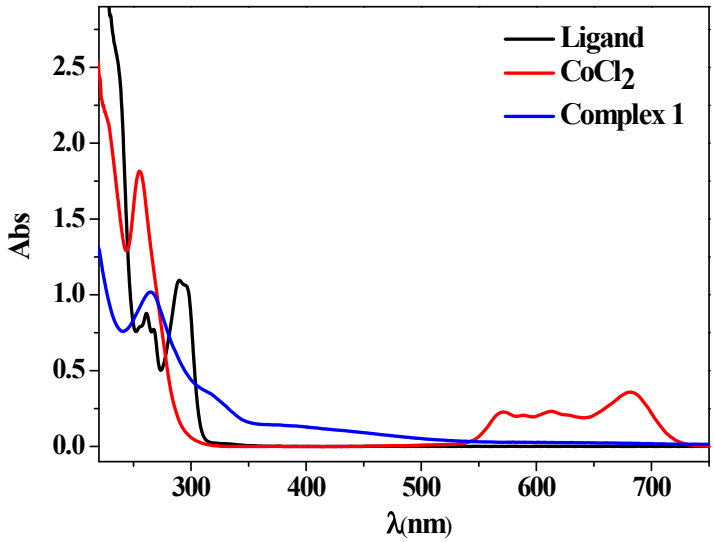

Fig. S1. The UV spectra of complex **1** and the related compounds in MeCN.

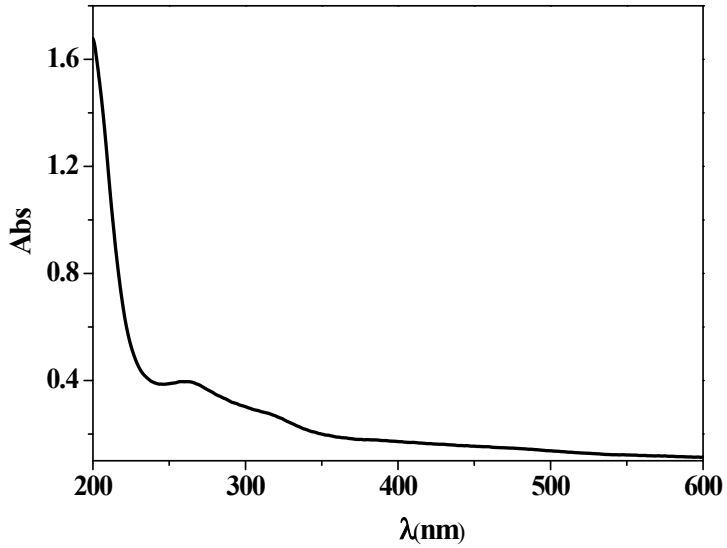

Fig. S2. The UV spectrum of 0.10 mM complex **1** in water.

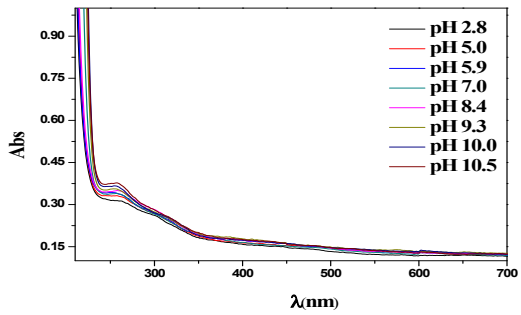

Fig. S3. The UV spectra of 0.10 mM complex **1** in 0.25 M phosphate buffered solutions at different pHs.

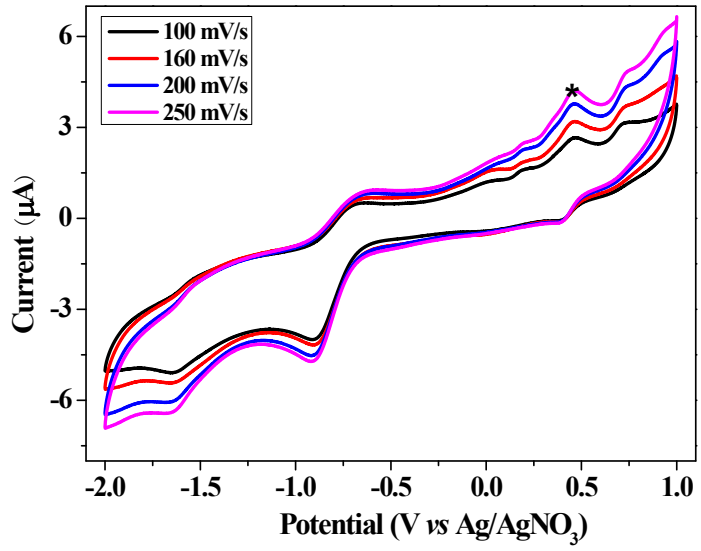

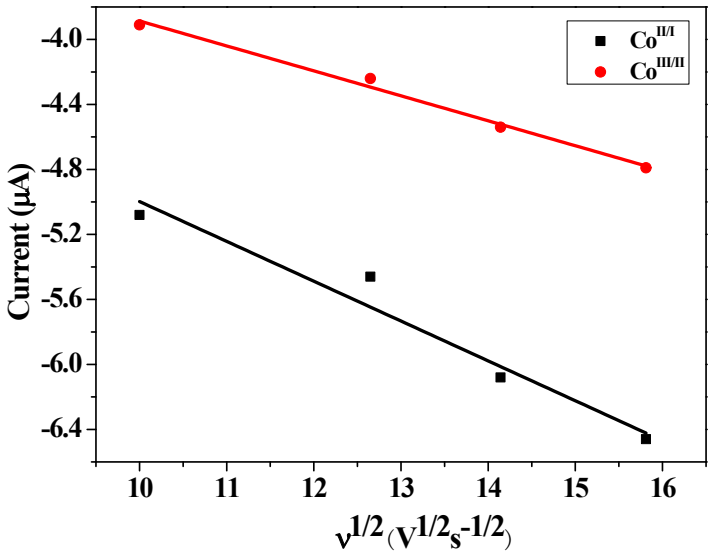

Fig. S4. Scan rate dependence of precatalytic waves at -1.58 V ($Co^{II/I}$) and 0.80 V ($Co^{III/II}$) for a 0.25 mM solution of complex **1** (0.10 M [n-Bu_4N]ClO_4), at scan rates from 100 to 250 mV/s.

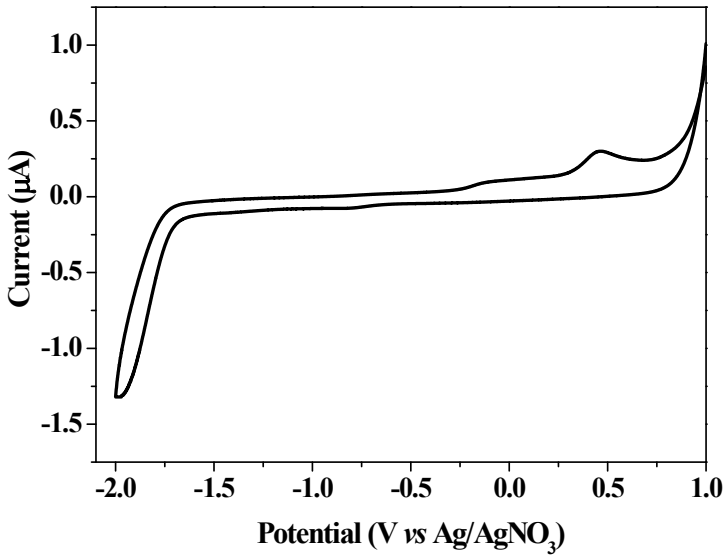

Fig. S5. CV of ligand (23 μM). Conditions: 0.10 M [n-Bu_4N]ClO_4 as supporting electrolyte, scan rate: 100 mV/s, glassy carbon working electrode (1 mm diameter), Pt counter electrode, $Ag/AgNO_3$ reference electrode.

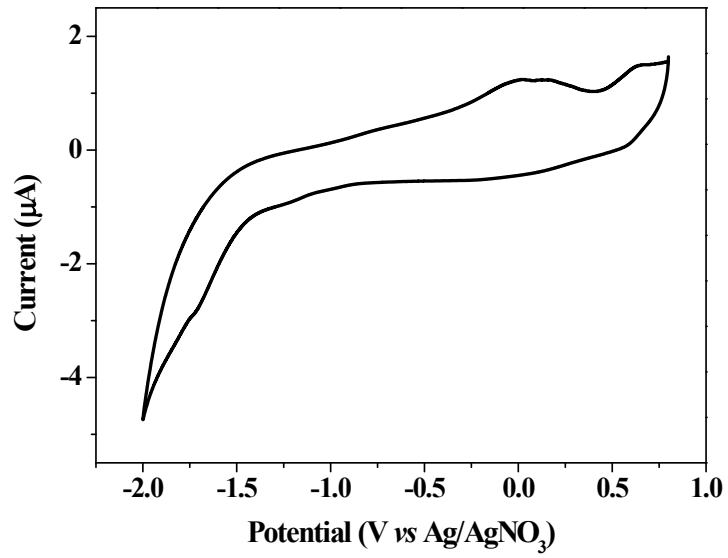

Fig. S6. CV of $CoCl_2 \cdot 6H_2O$ (23 μM). Conditions: 0.10 M [n-Bu_4N]ClO_4 as supporting electrolyte, scan rate: 100 mV/s, glassy carbon working electrode (1 mm diameter), Pt counter electrode, $Ag/AgNO_3$ reference electrode.

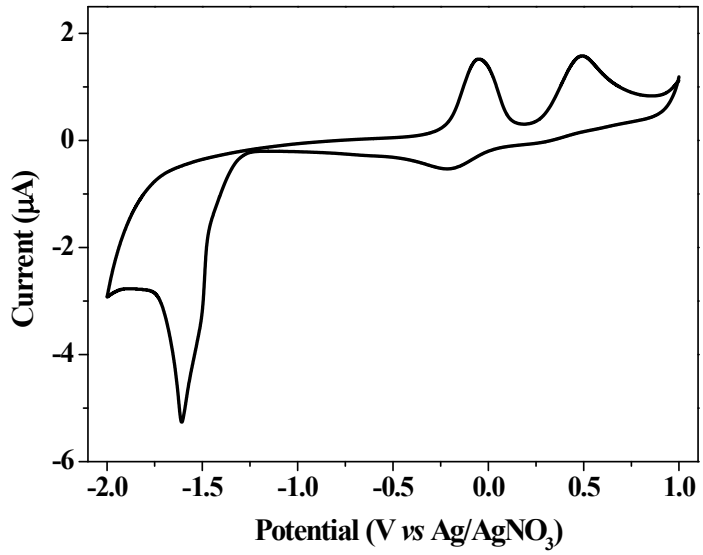

Fig. S7. CV of the mixture of $CoCl_2 \cdot 6H_2O$ (23 μM) + ligand (23 μM). Conditions: 0.10 M [n-Bu_4N]ClO_4 as supporting electrolyte, scan rate: 100 mV/s, glassy carbon working electrode (1 mm diameter), Pt counter electrode, $Ag/AgNO_3$ reference electrode.

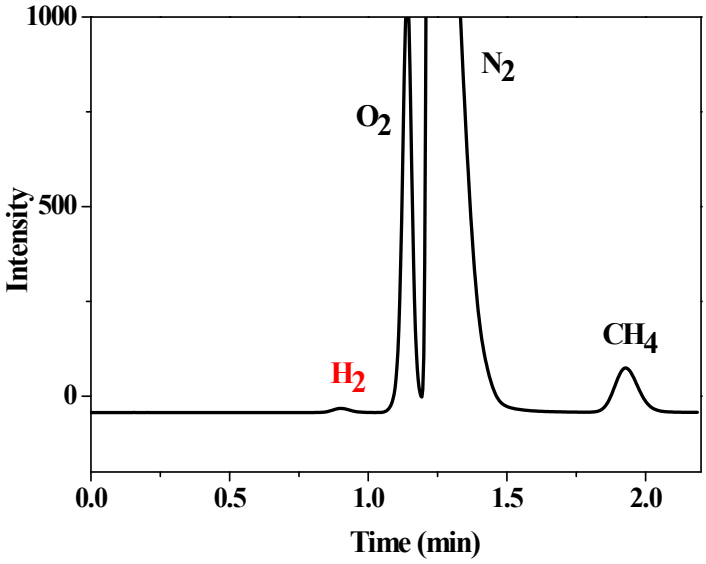

Fig. S8. GC traces after a 2-h controlled-potential electrolysis at −1.45 V *vs* Ag/AgCl of 4.0 μM complex **1** in DMF with 3.4 mM acid. A standard of CH_4 was added for calibration purposes.

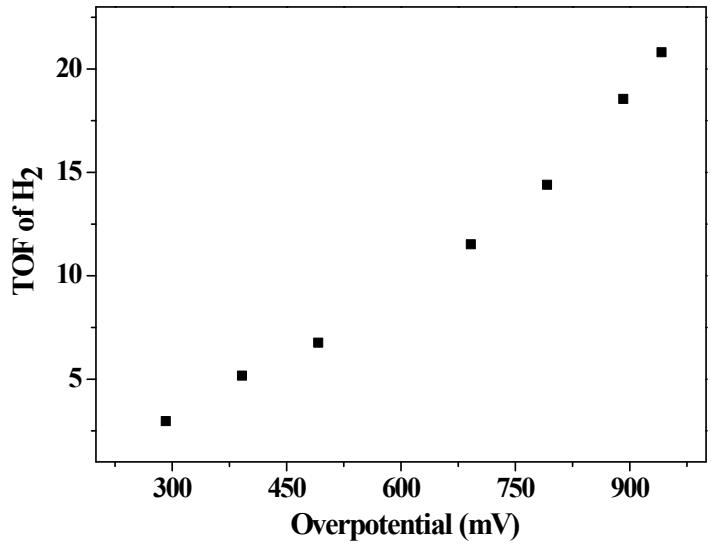

Fig. S9. Turnover frequency (mol H_2/mol catalysts/h) for electrocatalystic hydrogen production by complex **1** (0.25 μM) under a series of overpotentials.

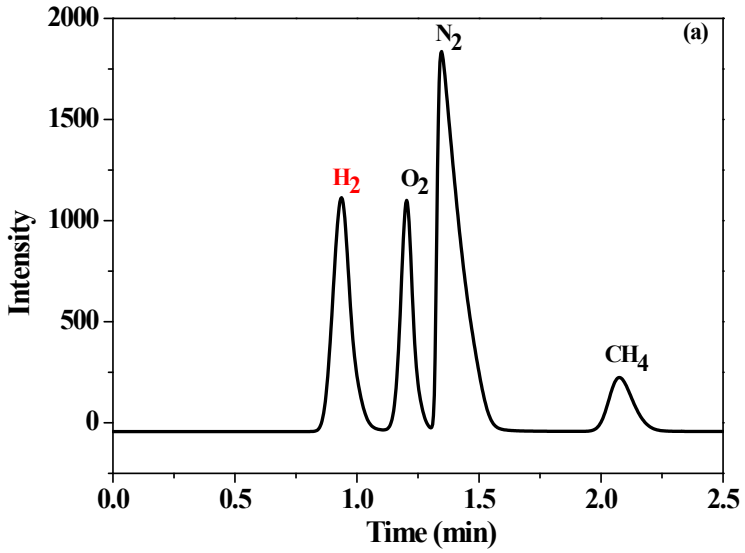

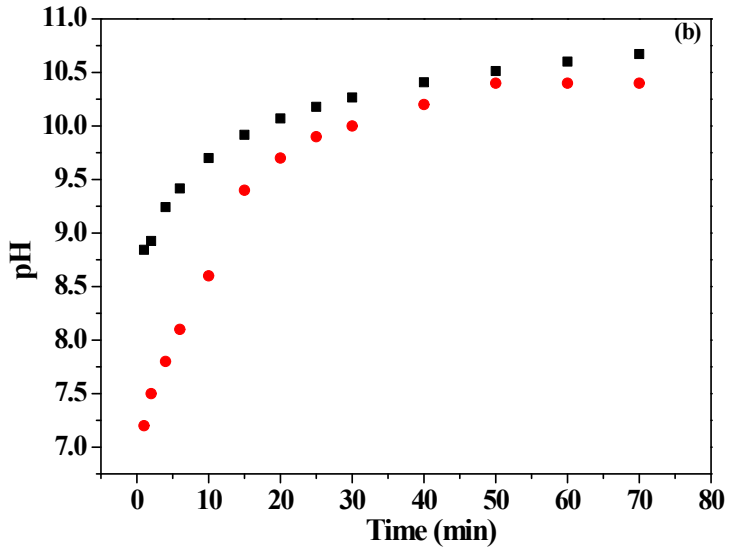

Fig. S10. (a) GC traces after a 1-h controlled-potential electrolysis at −1.45 V *vs* Ag/AgCl of 2.0 μM complex **1** in 0.25 M phosphate buffer, pH 7.0. A standard of CH_4 was added for calibration purposes. (b) Measured (black) and calculated (red) pH changes assuming a 100% Faradic efficiency of complex **1** during electrolysis. (the theoretical pH change over time can be calculated by the equation of $pH = 14 + \lg\frac{\sum It}{FV}$ where I = current (A), t = time (s), F = Faraday constant (96485 C/mol), V = solution volume (0.04 L)).

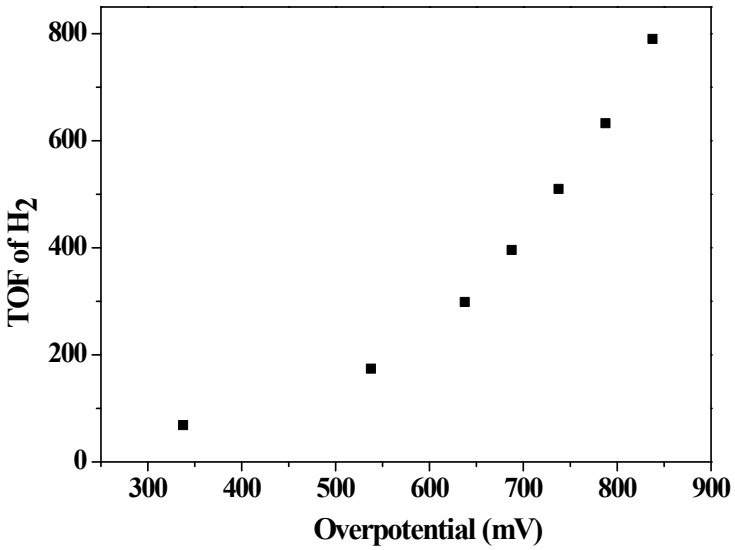

Fig. S11. Turnover frequency (mol H_2/mol catalysts/h) for electrocatalystic hydrogen production by complex **1** (2.0 μM) under a series of overpotentials (mV) at pH 7.0.

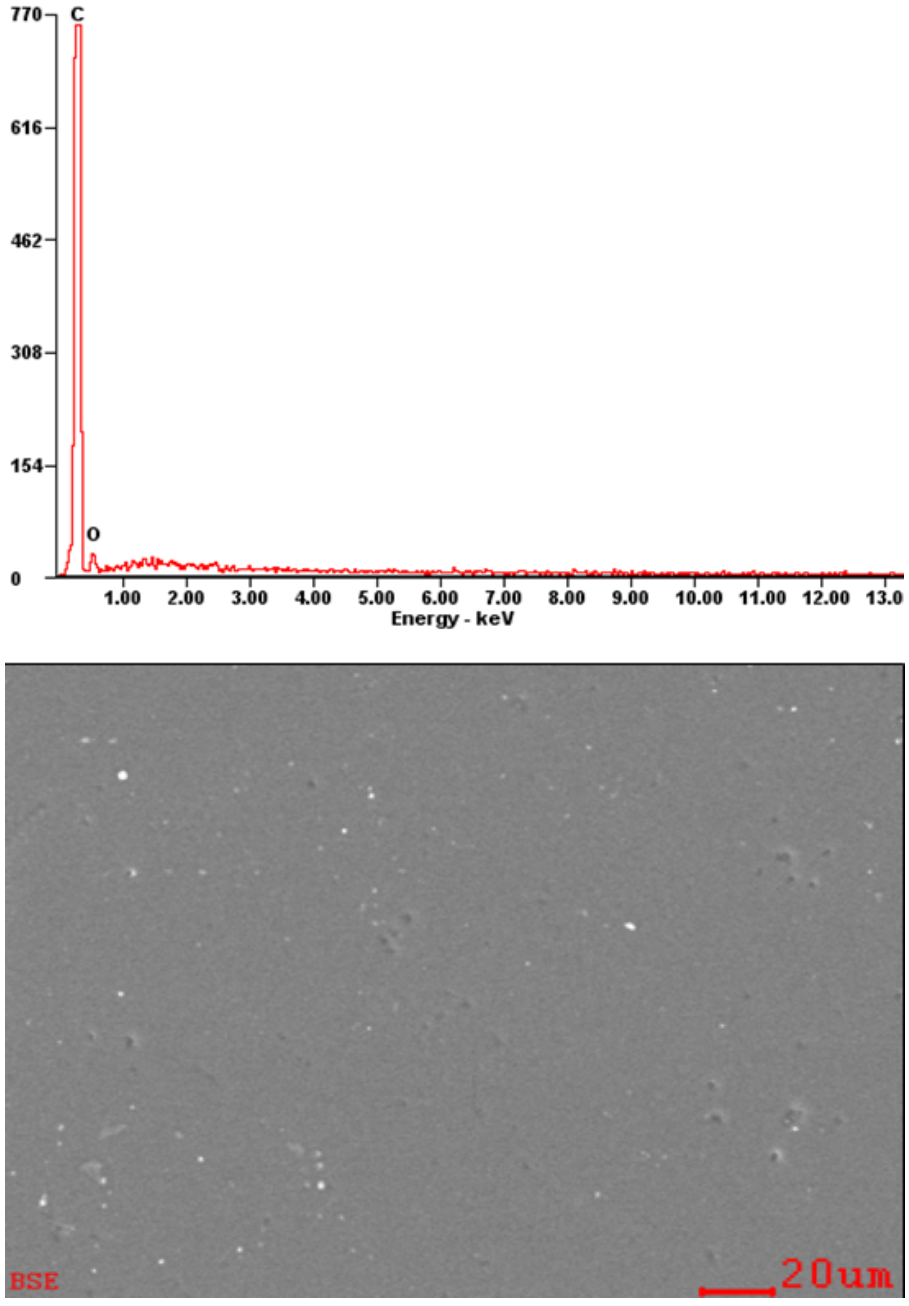

Fig. S12. EDS of a glassy carbon electrode after 3 h electrolysis. There was no significant change in the EDS after a 3 h electrolysis period.

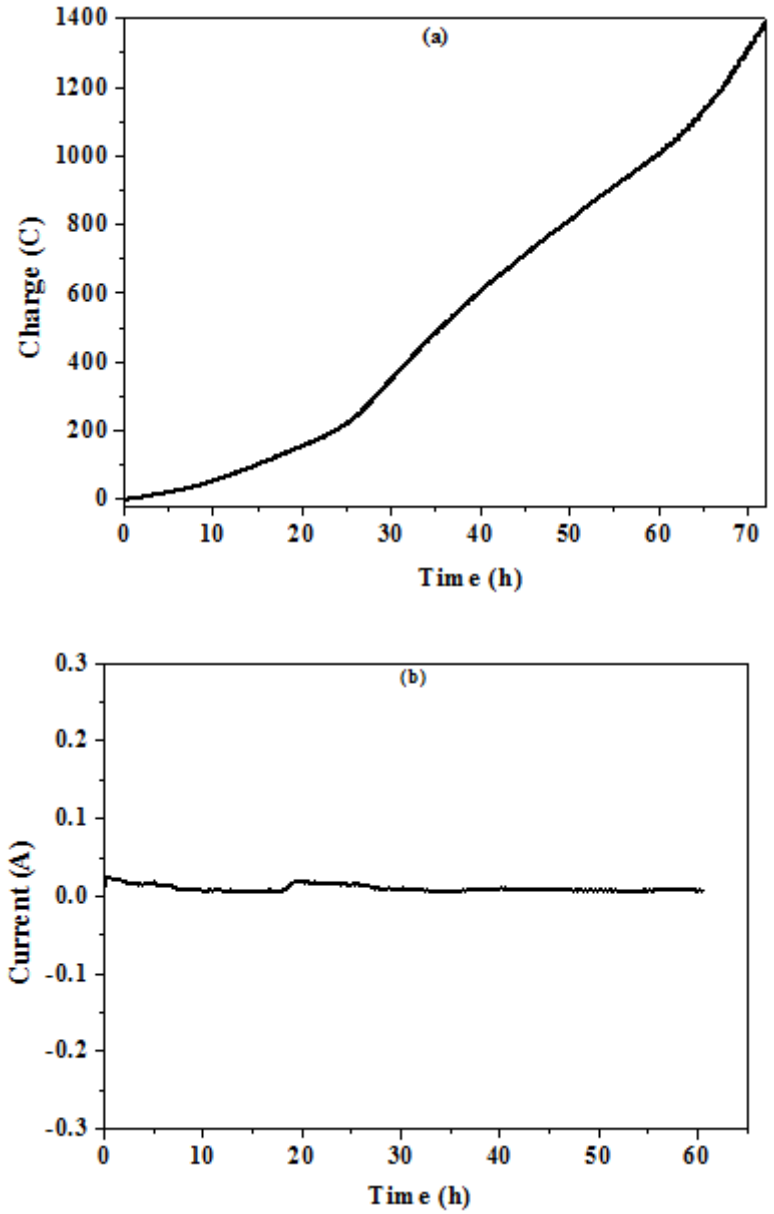

Fig. S13. (a) Extended controlled potential electrolysis of 4.5 μM complex **1**, showing charge buildup versus time with an applied potential of -1.45 V versus Ag/AgCl. (b) Catalytic current obtained upon controlled potential electrolysis with 4.5 μM complex **1**. Conditions: 0.25 M buffer solution, pH 7.0, GC working electrode (1.25 cm^2), Ag/AgCl in saturated KCl reference electrode, Pt wire counter electrode, 60 h.

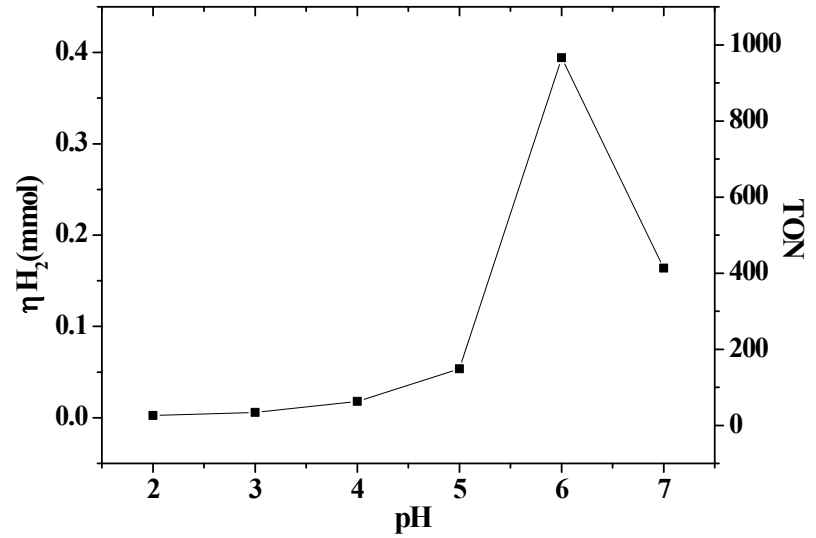

Fig. S14. Effect of pHs on different photocatalytic systems, containing 0.70 mM $Ru(bpy)_3Cl_2$, 0.08 M ascorbic acid and 0.10 mM complex **1**, under air.

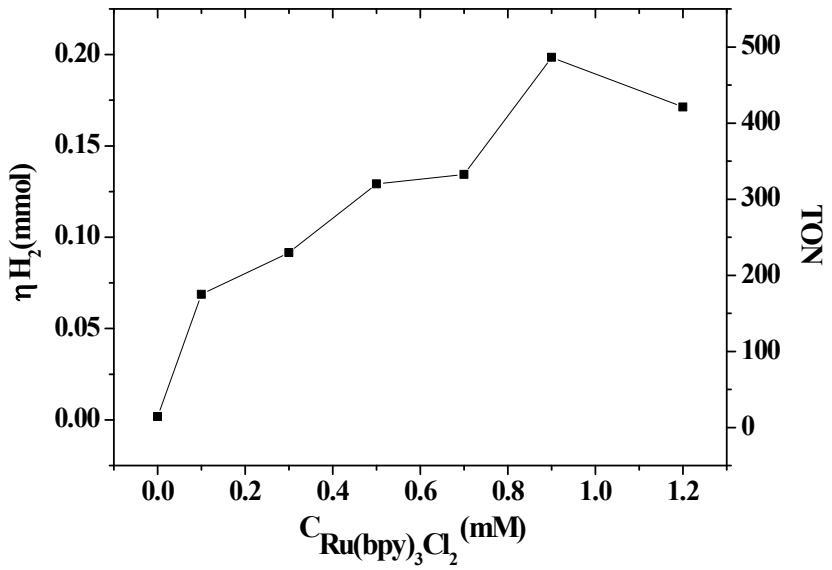

Fig. S15. Effect of addition of $Ru(bpy)_3Cl_2$ on different photocatalytic systems, containing 0.15 M ascorbic acid and 0.10 mM complex **1** at pH 6.0.

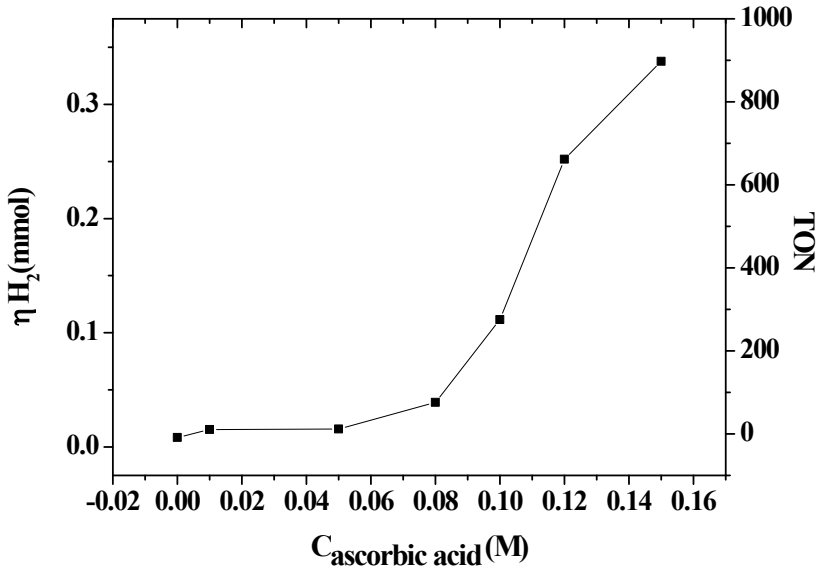

Fig. S16. Effect of addition of ascorbic acid on different photocatalytic systems, containing 0.70 mM $Ru(bpy)_3Cl_2$ and 0.10 mM **1,** at pH 6.0.

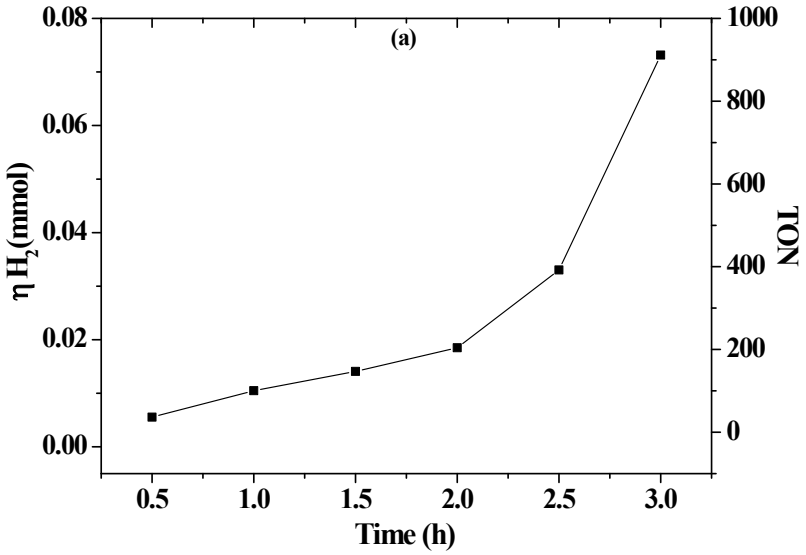

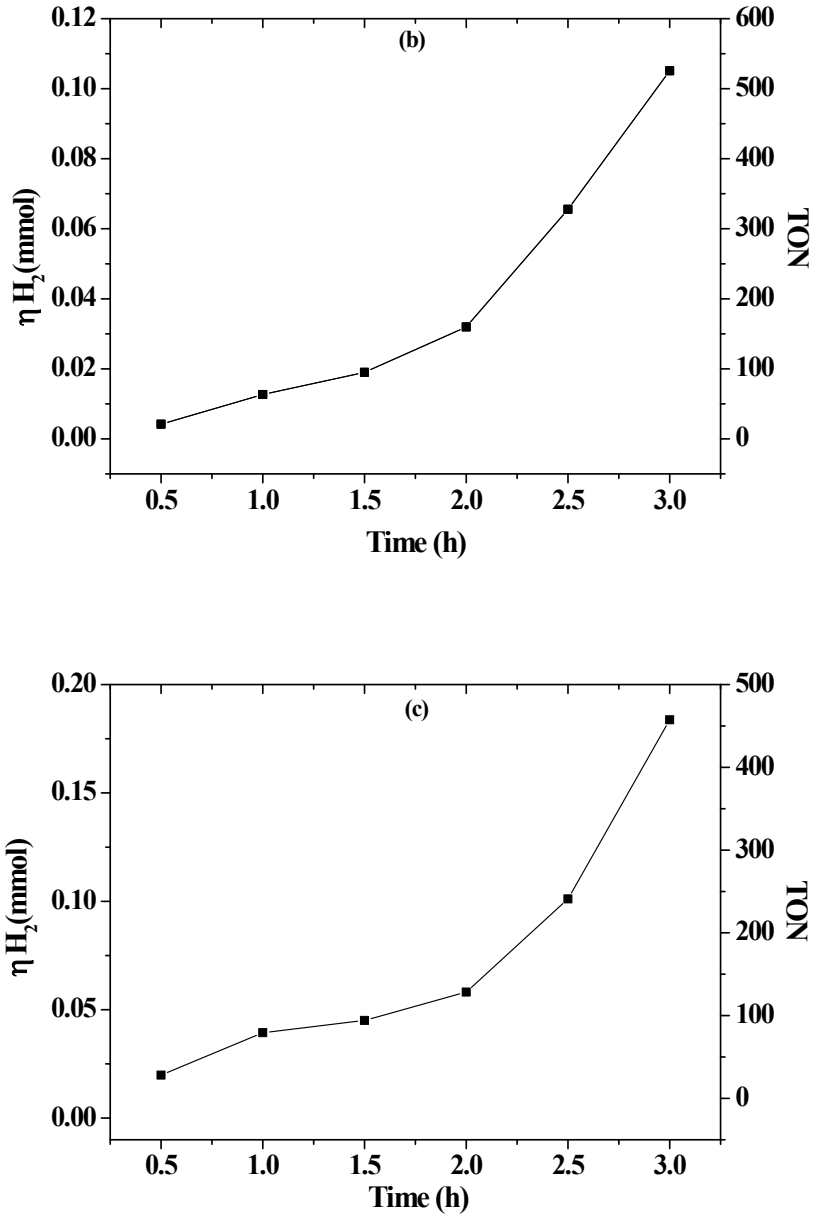

Fig. S17. Hydrogen evolution kinetics obtained upon continuous visible irradiation (λ = 469 nm) of 1.0 M buffer pH 6.0 solutions (4 mL) containing 0.90 mM $Ru(bpy)_3Cl_2$, 0.15 M ascorbic acid, and **1** at 0.02 mM (a), 0.05 mM (b), and 0.10 mM (c) concentration.

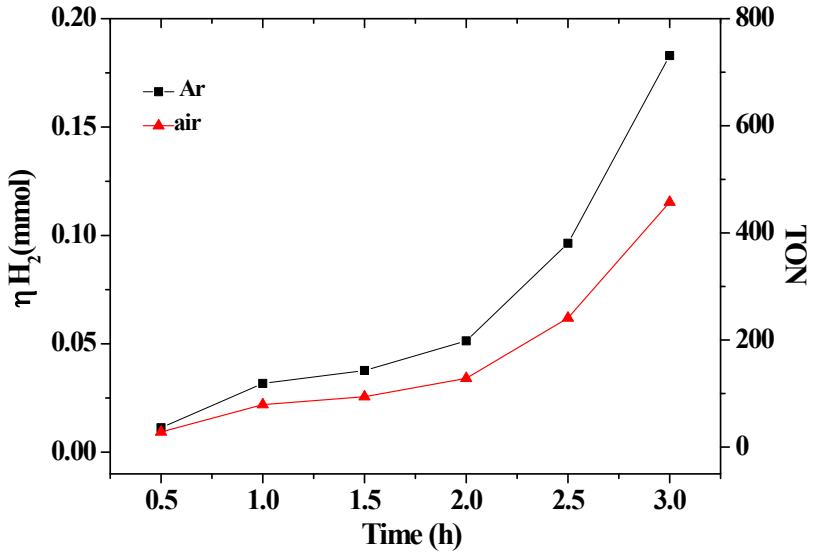

Fig. S18. Hydrogen evolution obtained upon continuous visible irradiation (λ = 469 nm) of pH 6.0 solutions (4 mL) containing 0.90 mM $Ru(bpy)_3Cl_2$, 0.15 M ascorbic acid, and 0.10 mM complex **1** under Ar (black trace), and air (red trace).

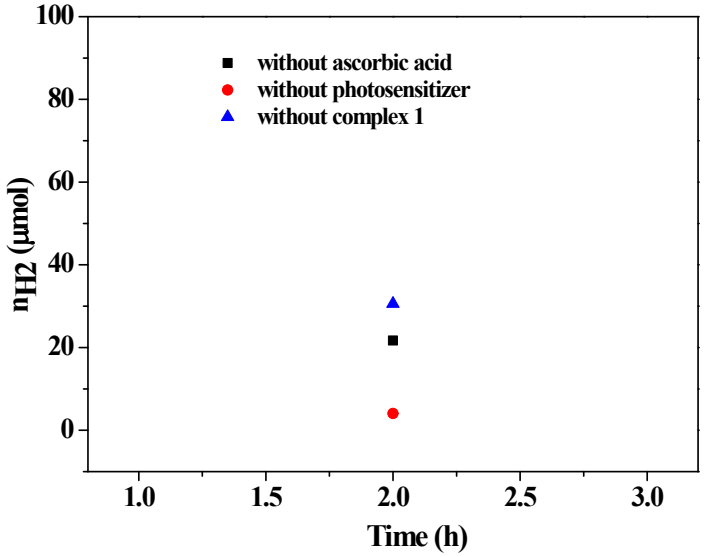

Fig. S19. Hydrogen evolution obtained upon visible irradiation (λ = 469 nm) of pH 6.0 solutions for 2 h, containing 0.30 mM $Ru(bpy)_3Cl_2$ and 0.10 mM complex **1** (black), 0.30 mM $Ru(bpy)_3Cl_2$ and 0.15 M ascorbic acid (blue), and 0.15 M ascorbic acid and 0.10 mM complex **1** (red).

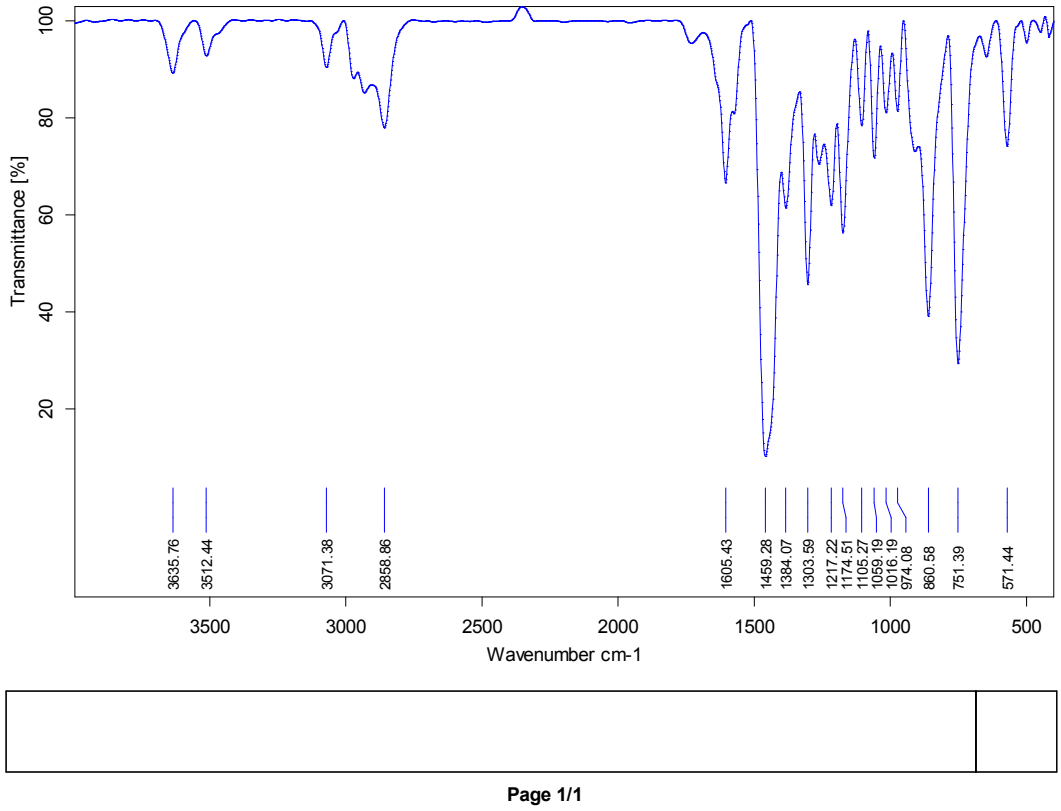

Fig. S20. IR spectrum of complex **1**.

$$TOF = \frac{\Delta C}{F \cdot n_1 \cdot n_2 \cdot t} = \frac{11.3016mC \times 3600}{96480C \cdot mol^{-1} \times 2 \times 0.084 \times 10^{-6} mol \times 120} = 20.79h^{-1}$$

Fig. S1. The calculation of TOF (DMF)

$$TOF = \frac{\Delta C}{F \cdot n_1 \cdot n_2 \cdot t} = \frac{0.4294C \times 3600}{96480C \cdot mol^{-1} \times 2 \times 0.08 \times 10^{-6} mol \times 120} = 789.6h^{-1}$$

Eq. S2. The calculation of TOF (Buffer, pH 7.0)

Table S1. Crystallographic data for **1**

Empirical formula	$C_{25}H_{26}N_2O_4Cl_5Co$
Formula weight	654.66
Temperature/K	296.15
Crystal system	monoclinic
Space group	$P2_1/c$
a/Å	14.659(3)
b/Å	20.200(4)
c/Å	9.5832(18)
α/°	90.00
β/°	100.056(4)
γ/°	90.00
Volume/Å^3	2794.1(9)
Z	4
ρ_{calc}g/cm^3	1.556
μ/mm^{-1}	1.127
F(000)	1336.0
Crystal size/mm^3	0.3 × 0.2 × 0.2
Radiation	MoKα (λ = 0.71073)
2Θ range for data collection/°	5.14 to 50.06
Index ranges	$-10 \leq h \leq 17$, $-24 \leq k \leq 21$, $-11 \leq l \leq 11$
Reflections collected	15110
Independent reflections	4932 [R_{int} = 0.0364, R_{sigma} = 0.0430]
Data/restraints/parameters	4932/0/336
Goodness-of-fit on F^2	1.072
Final R indexes [I>=2σ (I)]	R_1 = 0.0660, wR_2 = 0.2023
Final R indexes [all data]	R_1 = 0.0893, wR_2 = 0.2243
Largest diff. peak/hole / e Å^{-3}	0.56/-1.72

Table S2. The selected bond distances for complex **1**

Bond distances (Å)			
Co1-Co1[1]	2.9084(14)	Co1-N9	1.905(4)
Co1-O6	1.913(4)	Co1- N13	1.972(4)
Co1-O8	1.906(4)	Co1- Cl1	1.909(4)
Co1-Cl1[1]	1.916(4)		

Table S3. The selected bond Angles for complex **1**

Bond Angles(°)			
O8-Co1-O6	87.01(16)	Cl1[1]-Co1-Co1[1]	40.42(12)
O8-Co1-Cl1[1]	171.89(16)	Cl1-Co1-Co1[1]	40.60(12)
O8-Co1-Cl1	91.07(16)	Cl1-Co1-O6	89.02(17)
N9-Co1-Co1[1]	93.20(13)	Cl1-Co1-N13	93.08(17)
Co1 Cl1 Co1	98.98(17)	Cl1-Co1-Cl1[1]	81.02(17)